# BioID based proteomic screen identifies VDAC2 as a coordinator of Bid dependent apoptotic priming during mitosis.

Robert Pedley[1,2], Louise E. King[1,2], Venkatesh Mallikarjun[1,3], Pengbo Wang[4], Joe Swift[1,3], Keith Brennan[2], and Andrew P. Gilmore[1,2]*.

*Address*.
Faculty of Biology, Medicine and Health
Manchester Academic Health Science Centre
University of Manchester
Manchester, UK.

1. Wellcome Trust Centre for Cell-Matrix Research
2. Division of Molecular & Clinical Cancer Sciences
3. Division of Cell Matrix Biology and Regenerative Medicine
4. Present address, Cancer Research UK Manchester Institute.

*Correspondence to:
Dr. Andrew P. Gilmore
Wellcome Centre for Cell-Matrix Research
Faculty of Biology, Medicine and Health
A.3034 Michael Smith Building
University of Manchester
Oxford Road
Manchester M13 9PT
Tel. 0161 275 3892
FAX. 0161 275 1505
Email agilmore@manchester.ac.uk

## Abstract

Apoptotic priming refers to the proximity of cells to outer mitochondrial membrane permeabilisation (MOMP), the point of apoptosis commitment. Variations in priming are important for how both normal and cancer cells respond to chemotherapeutic agents. Individual cells adjust their level of priming in response to changing circumstances, such as genomic damage. How changes in apoptotic priming are dynamically coordinated by Bcl-2 proteins remains unclear. We have previously demonstrated that the Bcl-2 protein, Bid, becomes phosphorylated as cell enter mitosis, increasing priming. To understand how cells coordinate dynamic changes in priming, we have performed an unbiased proximity biotinylation (BioID) screen using Bid as bait. This identified several potential regulatory proteins outside the core Bcl-2 family. In particular we found VDAC2 to be essential for Bid phosphorylation dependent changes in apoptotic priming during mitosis. These results show the importance of dissecting the wider Bcl-2 interactome, and identify a key scaffold protein coordinating dynamic changes in single cell priming.

## Introduction

Most cells respond to an apoptotic stimulus through mitochondrial outer membrane permeabilisation (MOMP) [1]. MOMP releases cytochrome *c* into the cytosol to initiate caspase activation. Following MOMP, cell death proceeds with largely invariant kinetics [2]. However, whether or not cells undergo MOMP following an apoptotic stimulus shows significant heterogeneity, both within a cell population as well as between different cells and tissues [3-5]. Apoptotic priming refers to how close a cell lies to MOMP, and therefore its subsequent response to damage [6,7]. Indeed, apoptotic priming of cancer cells can predict how a patient might respond to chemotherapy [8,9]. However, how variations in apoptotic priming are established, and how it changes dynamically, remain poorly understood.

MOMP is regulated through interactions between Bcl-2 family proteins [10,11]. The Bcl-2 family comprise: pro-apoptotic multidomain proteins Bax and Bak, which form the pores that drive MOMP; anti-apoptotic proteins, such as Bcl-XL, Bcl-2, and Mcl-1, that suppress MOMP by sequestering pro-apoptotic proteins; and the BH3-only proteins, which regulate the activity of the other two groups. BH3-only proteins may be activators or sensitizers. Activators, including Bim and Bid, bind Bax and Bak directly to initiate MOMP. Activator BH3-proteins can also be sequestered by anti-apoptotic Bcl-2 proteins, but are released by the sensitizer subgroup of BH3-only proteins, such as Bad, which compete for binding [12]. Thus, variation in the expression and interaction of the different Bcl-2 family subgroups can set the level of priming, subtle changes in which have profound implications for processes such as embryonic development [13].

Apoptotic priming can be highly dynamic, adjusting within minutes in response to changes in survival signaling [7]. Mitosis represents part of the cell cycle where dynamic changes in apoptotic priming are precisely controlled [14]. Upon entry to mitosis, cells become primed so that those that fail to divide correctly are eliminated. However, apoptosis is initially suppressed for a period of time to allow spindle assembly to occur. Once cells satisfy the Spindle Assembly Checkpoint (SAC), they enter anaphase and reduce priming to allow cell division to occur without dying first. If cells fail to satisfy the SAC sufficiently quickly, they will be eliminated through

apoptosis. Thus, mitosis provides an excellent and unique model for understanding how cells dynamically adjust apoptotic priming within precise temporal boundaries. The shift in apoptotic priming seen upon mitotic entry is linked to both post-translational modifications to several Bcl-2 proteins[15-20] and changes in their expression, driven in part by Myc [21,22]. In particular, we have shown that the BH3-only protein Bid is phosphorylated as cells enter mitosis to increase priming [20], whilst others have shown that the slow degradation of Mcl-1 through mitosis determines how long a cell has to satisfy the SAC to avid apoptosis [16,23].

How mitosis coordinates temporal adjustments to apoptotic priming is not clear, but has important implications for how cells respond to anti-mitotic drugs. Anti-mitotic drugs exploit the induction of apoptosis in cells arrested during mitosis and they have become an essential component of cancer therapy since the introduction of Taxol in the early 1990's [24]. However it is clear that cancers can become resistant to anti-mitotics, and cells can exit mitosis without accurately dividing, termed slippage [3,25]. Slippage occurs through the gradual degradation of cyclin B in the absence of correct spindle attachment. For a cell to die before slippage, it must reach the threshold for MOMP before cyclin B levels decline far enough to result in slippage [25]. Determining the mechanisms coordinating dynamic changes in apoptotic priming at mitochondria may allow us to improve the response to anti-mitotics.

To this end, we have performed an unbiased proteomic screen based upon proximity-dependent biotin identification (BioID)[26], using Bid as bait. Using this approach, we identify a number of possible regulatory molecules controlling Bid function. In particular we find that the outer membrane porin, VDAC2, is critical for cells to adjust priming in response to Bid phosphorylation. Thus, this approach identifies mitochondrial proteins involved in co-ordinating Bcl-2 dependent changes in apoptotic priming.

## Results

*Breast cancer cells show wide variations in apoptotic priming during a prolonged mitosis.*

We wanted to use the increased sensitivity of cells to apoptosis during a prolonged mitosis to identify mitochondrial proteins involved in dynamically adjusting priming. Previous studies have shown that there is considerable inter- and intra-line variability in the response of cells to anti-mitotic drugs[3]. Initially we followed five different cell lines, four cancer lines (MCF7, BT-474, SK-BT-3, MDA-MB-231) and one normal (MCF10A). We used live imaging on unsynchronised, sub-confluent cells in the presence or absence of taxol to determine single cell fate profiles over 65 hours, quantifying entry into mitosis, normal division, apoptosis and slippage (Fig. S1). There was very little apoptosis in untreated cells. However, the five breast lines show wide variations in their response to prolonged mitosis (Fig. 1A, B). In the presence of taxol, MCF7, BT474, SK-BR-3 and MCF10A cells predominantly underwent apoptosis during mitosis (Fig. 1B, C). Conversely, triple negative MDA-MD-231 cells were prone to slippage. Interestingly, in the presence of taxol, little apoptosis was seen prior to mitosis. In all the lines, taxol significantly increased the time in mitosis compared with untreated cells, although this showed wide variations both within and between lines (Fig.1D).

We have previously shown that the BH3-only protein, Bid, was phosphorylated in mitosis [20], which was linked to the sensitivity of colon carcinoma cells to taxol-induced apoptosis [20]. We asked if Bid phosphorylation was linked to sensitivity of the breast cell lines to death in mitosis. Mouse and human Bid are phosphorylated on functionally equivalent amino acids, serine 66 in mouse and 67 in human [20]. However, whereas phosphorylated mouse Bid (mBid) shows a mobility shift by SDS-PAGE, human Bid does not. We therefore expressed an mBid-GFP fusion in the human breast lines in order to observe Bid phosphorylation. Mitotic cells for each line were collected by culturing the cells overnight in Nocodazole, and shaking off those in mitosis. mBid-GFP from mitotic cells was compared with that from unsynchronised cells by SDS-PAGE and immunoblotting (Fig.1E). Despite the variation in response to taxol, all five lines showed a slower migrating band indicative of mBid-GFP phosphorylation in mitosis.

*Bid phosphorylation adjusts the set point of apoptotic priming during mitosis in breast cancer cells.*

To determine whether Bid phosphorylation sets priming in breast cancer cells, we used a lentiviral approach to simultaneously knock down endogenous human Bid (hBid) whilst expressing mBid-GFP, using an ubiquitin promoter to express at levels similar that of endogenous Bid [20]. We used MCF7 cells, which predominantly undergo apoptosis if mitotic exit is delayed. Stable MCF7 lines were generated that expressed the hBid shRNA, alone or in conjunction with wildtype mBid-GFP (mBidWT-GFP), or mBid-GFP variants where S66 had been substituted to alanine (mBidS66A-GFP), or where the BH3-domain required for interacting with other Bcl-2 proteins had been made non-functional (mBidG94E-GFP). The lines were selected for similar expression levels by FACS (Fig. 2A). Both mBidWT-GFP and mBidG93E-GFP showed the slower migrating phosphorylated form in mitotic cells as expected (Fig. 2A). Endogenous hBid expression was knocked down more than 70% (Fig. 2B).

We next performed single cell fate profiling to compare parental MCF7 (WT MCF7) cells with those expressing shBid alone or with the mBid-GFP variants. In the absence of taxol there was no difference between the lines, either for apoptosis or time in mitosis (Fig2C, Fig. S2A,B,C). Flow cytometry confirmed that the different mBid-GFP variants had no impact on the proportion of cells in each cell cycle stage (Fig. S2F). Thus, Bid expression, phosphorylation and apoptotic function do not affect normal cell cycle progression. However, in the presence of taxol, Bid knock down shifted MCF7 cell fate from apoptosis to slippage (Fig. 2C; Fig S2A, D). This distribution of cell fate was corrected by expression of mBidWT-GFP, but not by either mBidS66A-GFP or mBidG94E-GFP. Thus, Bid expression, phosphorylation and pro-apoptotic function are required for the temporal adjustment of priming in MCF7 cells seen during mitosis.

Bid phosphorylation still occurred in mitotic MDA-MB-231 cells, even though these appeared largely resistant to taxol. We therefore wondered whether Bid phosphorylation still adjusted the priming set point when these entered mitosis. To test this we generated stable MDA-MB-231 lines expressing shBid with either mBidWT-GFP, mBidS66A-GFP or mBidG94E-GFP (Fig. S3A). As with MCF7, the Bid variants by themselves did not alter progression though normal mitosis (Fig.

S3B,C,D,E). However, in the presence of taxol there was a reduction in the proportion of MDA-MB-231 cells that underwent apoptosis in mitosis in the lines expressing Bid-S66A-GFP or BidG94E-GFP. Thus, although the baseline of apoptotic priming in MDA-MB-231 cells is much higher than that of MCF7, they still show Bid dependent sensitisation upon mitotic entry.

Although Bid phosphorylation adjusts priming, there is still considerable heterogeneity in single cell outcomes for both MCF7 and MDA-MB-231. Other Bcl-2 proteins undergo changes in expression and post-translational modifications during mitosis, and cell fate will represent the summation of multiple events. To examine this, we treated the MCF7 and MDA-MB-231 lines with a combination of taxol and the BH3-mimetic, ABT-737, which inhibits anti-apoptotic Bcl-XL, Bcl-2 and Bcl-W. ABT-737 alone did not impact on normal mitosis but did have a significant impact on the outcome of a prolonged mitosis. In MCF-7 cells, ABT-737 negated the impact of Bid phosphorylation on priming (Fig. 2E). MDA-MB-231 cell fate was dramatically shifted toward apoptosis by the BH3-mimetic (Fig. S3F). In both lines, the data indicate that dynamic adjustment of priming in mitosis is dependent upon anti-apoptotic Bcl-2 proteins. Furthermore, shifting the cell fate away from slippage resulted in cells spending less time in mitosis (Fig.2F, Fig.S2E, Fig.S3G).

Together, these data highlighted Bid phosphorylation as a common mechanism by which mitotic cells dynamically adjust apoptotic priming, even when the overall outcomes appear quite different. We therefore decided to use this observation to identify regulatory complexes controlling temporal changes in priming using an unbiased proteomic strategy.

*BioID based proximity labelling allows identification of Bid interaction partners in live cells.*

BioID is a powerful approach to identify protein interactions in live cells and has been successfully applied to interrogate protein complexes within the centrosome, the nuclear pore, and cell-ECM adhesions [26-29]. The strategy involves expressing a bait protein as a fusion with the *E.coli* biotin ligase BirA containing a R118G amino acid substitution along with a myc epitope tag (from here on referred to as BirA*). In the

presence of excess Biotin in the culture media, BirA* fusions generate reactive biotinyl-5'-AMP that can label primary amines. The half-life of the reactive biotinyl-5'-AMP limits the effective labelling radius to ~20 nm [26]. Labelled proteins are isolated by streptavidin affinity purification (Fig.4A). As labelling occurs *in situ*, it is particularly useful for interrogating complexes that might be disrupted by detergents used in cell extraction, a known issue with Bcl-2 protein interactions [30,31]. We therefore undertook a BioID strategy to identify Bid interactions in live cells.

To validate the functionality of mBid-BirA* fusions, we compared the pro-apoptotic function of truncated Bid (tBid) fused to either eYFP or BirA*. Both induced similar levels of apoptosis when transiently expressed in HEK-293T cells (Fig.3B). GFP-BirA* did not induce apoptosis. We next validated tBid-BirA* dependent labelling in the presence of Biotin. HEK-293T cells transiently expressing tBid-BirA* or BirA* were grown in normal media or media supplemented with Biotin for 18 hrs. Whole cell lysates were probed with strepavidin or anti-myc (Fig.3C). The expressed fusions proteins both showed self-labelling in the presence of Biotin. To determine if tBid-BirA* could label known binding partners, we transiently expressed GFP-BclXL in HEK-293T cells, either alone or with tBid-BirA*, cultured the cells in the presence of Biotin, and subjected lysates to strepavidin affinity purification. The whole cell lysates (WCL), the unbound and bound fractions were then blotted for GFP or biotin (Fig.3D). GFP-BclXL was isolated only when it was co-expressed with tBid-BirA*. Finally, we used fluorescence microscopy to visualise biotin in cells expressing either tBid-BiA* or BirA* (Fig.3E). Only cells expressing either tBid-BirA* or BirA* were positive for biotin. Notably, the tBid-BirA* expressing cells showed mitochondrial localisation of biotin.

*Proximity biotin labelling identifies Bid interacting partners in mitotic cells.*

In order to identify mitosis specific Bid interacting partners, we utilised label free mass-spectroscopy using HeLa cells stably expressing mBid-BirA* (Fig.4A). HeLa cells were chosen because they show Bid phosphorylation in mitosis as well as allowing robust enrichment of mitotic cells, important as dilution of the mitotic population would impair identification of interactions.

BirA* tagged bait proteins were expressed from a lentivirus co-expressing tagBFP downstream of a T2A cleavage sequence. As tagBFP was expressed at a 1:1 ratio with each BirA* fusion, we could select stable lines with equivalent expression of each. We generated stable HeLa lines expressing mBidWT-BirA*, mBidS66A-BirA*, mBidG94E-BirA* or venus-BirA* (Fig.4B, Fig.S4A,B). Each line, either arrested in mitosis or left unsynchronised, was maintained in biotin containing media for 16 hours, a time frame that allowed significant enrichment for labelling in mitosis (Fig. S4C). Labelled proteins were isolated by Streptavidin affinity purification, analysed by LC-MS/MS, and quantified using Progenesis QI. We performed three independent experiments, typically identifying >400 hundred proteins within each sample, with the bait being one of the most abundant (Fig.4C). Enrichment of proteins within each mBid-BirA* sample was determined by comparison with venus-BirA*.

For proteins enriched in mBid-BirA* expressing cells, we applied multiple criteria to determine which to prioritise for further analysis. We initially compared the sequence coverage of each and their relative representation in the contaminant repository for affinity purification (CRAPome), which collates proteins most often found within negative control AP-MS data (Fig.4D)[32]. Several proteins of interest only appeared in two out of the three repeats. Of these, Bax, was identified in mBidWT-BirA* cells and enriched in mitosis. Other candidates within this category, including kinases and signalling enzymes, are of interest with regard to Bid regulation, and will be the subject of future studies. However, for the present study we restricted selection to proteins detected in all three repeats, resulting in a significantly shorter list of candidates for validation (Table 1A and B).

Falling within these strict criteria was the mitochondrial porin, VDAC2, which has been previously linked to Bax and Bak function [33-36]. We compared enrichment of VDAC2 in unsynchronised and mitotic cells expressing either mBidWT-BirA*, mBidS66A-BirA* or mBidG94E-BirA* (Fig.4E). VDAC2 was enriched in mitotic cells expressing the mBidWT-BirA* bait compared to unsynchronised cells. Furthermore, VDAC2 enrichment was significantly less in mitotic cells expressing either BidS66A-BirA* or BidG94E-BirA*. Other proteins identified in all three repeats did not show mitosis or Bid variant specific enrichment (Fig.4E). For example, mtHsp70 showed no differences between lines expressing mBidWT-BirA* or the S66A and G94E variants. Notably, VDAC1, which is ~10-fold more abundant than VDAC2 in HeLa

cells [37], was not enriched. As quantification was performed using only non-conflicting peptide sequences, any sequence similarity between VDAC isoforms was not a confounding issue.

These results show that proximity labelling can identify potential candidate components of cell-cycle stage specific Bcl-2 protein complexes.

*VDAC2 is required for Bid phosphorylation dependent priming in mitosis.*

We next asked if VDAC2 influenced apoptotic priming in mitotic cells. To do this, we employed a knock out (ko) strategy in the MCF7 cells, where the response to taxol was influenced by Bid phosphorylation (Fig. 2C). MCF7 cells were transfected with a CRISPR/Cas9 targeting vector with a guide sequence to the start of the protein-coding region of the *VDAC2* gene, and single cell clones isolated. Three clones, termed D11, D6 and D4, were identified containing insertions or deletions within the *VDAC2* gene (Fig.5A). MCF7 cells have three copies of *VDAC2*. Sequencing indicated that D11 had all three copies containing frame-shifting insertions, D6 had two frame shift insertions and one WT allele, and D4 two frame shift insertions and one allele with a 3 bp deletion within the coding sequence.

We performed cell fate analysis to compare WT MCF7 cells to the three VDAC2 ko lines (Fig.5B). There were no differences in how the three VDAC2 ko lines progressed through normal mitosis compared to WT cells. However, compared to WT cells all three VDAC2 ko lines showed a shift toward slippage vs. apoptosis when mitosis was prolonged with taxol (Fig.5B). Although many VDAC2 deficient cells still underwent cell death during prolonged mitosis, the proportion undergoing slippage was comparable to that seen in the shBid MCF7 cells, or those expressing mBidS66A or mBidG94E (cf. Fig.2C). To confirm the effect was due to the loss of VDAC2, we stably re-expressed VDAC2 tagged with a V5 epitope in the MCF7 D11 line. We utilised a lentivirus with an ubiquitin promoter to ensure that we did not overexpress VDAC2-V5, and a T2A cleavage peptide with a downstream tagRFP for selection by FACS. VDAC2-V5 localised to mitochondria (Fig.5C). Cell fate profiling showed that expression of VDAC2-V5 rescued D11 cells so that they now showed the same level of apoptosis in mitosis in taxol as parental MCF7 cells (Fig.5E, Fig.S5).

Finally, we asked if VDAC2 was required for coupling Bid phosphorylation to mitotic priming. The D11 line was infected with the shBid lentivirus, or shBid virus co-expressing mBidWT-GFP, mBidS66A-GFP or mBidG94E-GFP (Fig.5C). Interestingly, BidWT-GFP and BidG94E-GFP were still phosphorylated in D11 cells arrested in mitosis, indicated by the mobility shift by SDS-PAGE (Fig.5D). We performed cell fate profiling in the presence or absence of taxol and/or ABT-737, comparing each mBid-GFP line to WT cells, the D11 ko and the D11-VDAC2-V5 (Fig.S5). Knock down of Bid had no further effect on the level of apoptosis in taxol beyond that already brought about by VDAC2 ko (Fig.5E). mBid-GFP, mBidS66A-GFP or mBidG94E-GFP expressing D11 cells all showed the same proportion of death vs. slippage in taxol as the D11 VDAC2 ko alone (Fig.5E). Furthermore, this level of death in mitosis was comparable to WT MCF7 cells infected with the shBid lentivirus (cf. Fig.2, Fig.S2). Apoptosis in all lines was restored to the level of WT MCF7 cells by treating with ABT-737 along with taxol. ABT-737 alone did not induce any significant level of apoptosis.

Together, the data presented here show that VDAC2 couples apoptotic priming in mitosis to Bid phosphorylation. Thus, VDAC2 is a necessary scaffold for coordinating the temporal regulation apoptotic sensitivity seen in mitotic cells.

## Discussion

The mechanistic understanding of apoptosis obtained over the past three decades has ultimately led to novel drugs directly targeting Bcl-2 protein interactions to therapeutically manipulate mitochondrial priming. However, it is still unclear how cells dynamically adjust their level of mitochondrial priming in reaction to changing internal and external signals, a key determinant for how cells will respond to chemotherapeutic drugs. Here we employed an unbiased proteomic approach to identify proteins that control dynamic changes in priming during mitosis, a clinically important chemotherapy target, and identify VDAC2 as a coordinator of dynamic mitochondrial priming in mitotic cells.

Our strategy was based on previous findings showing that cells adjust priming as they enter mitosis. Cell death following delayed mitotic exit is Bcl-2 protein dependent, and several Bcl-2 family members undergo mitosis specific post-

translation modifications, including Bcl-2, Bcl-XL, Mcl-1 and BimEL [17-20]. Progressive degradation of Mcl-1 during mitosis is of particular significance as it leads to loss of anti-apoptotic function when anaphase is delayed, ultimately resulting in MOMP. However, cells become sensitised to this loss of anti-apoptotic Bcl-2 protein upon mitotic entry. Thus, in both MCF7 and MDA-MB-231 cells, BH3-mimetics had little impact on cell survival in interphase, but increased cell death once taxol-treated cells passed G2/M, as well as decreasing the time in mitosis before dying. We hypothesised that a specific post-translational modification could identify mechanisms coordinating changes in mitochondrial priming associated with mitosis.

We have previously reported that full-length Bid is phosphorylated on serine 66 (67 in human) during mitosis[21]. Our data suggest that this phosphorylation does not convert Bid into a direct activator of MOMP, as with caspase 8 cleavage. Rather, phosphorylated full-length Bid appears to function as a sensitiser, reversibly increasing priming in mitosis. We therefore reasoned that we could use BioID for *in situ* proximity labelling to identify Bid vicinal proteins in mitosis, and use this is a model to elucidate how post-translational modifications of Bcl-2 proteins coordinate changes in mitochondrial priming. Following labelling, biotinylated proteins can be subjected to stringent affinity purification. This allows extraction of integral mitochondrial membrane proteins that might not be isolated under conditions necessary for more traditional protein-protein interactions approaches, such as co-immune precipitation. Furthermore, this approach avoids known issues with detergents on Bcl-2 protein interactions [28]. The compromise for these benefits is that BioID has the potential to label non-specific proximal proteins [26]. However, we mitigated against detecting false positives by comparative analysis of WT, S66A and G94E Bid variants, all of which showed equivalent subcellular localisation, but had distinct effects on mitochondrial priming[24,42].

Of the proteins enriched in mBid-BirA* cells relative to venus-BirA* controls, VDAC2 was notable because it was enriched specifically in mitotic cells, and then only when Bid was both functional and able be phosphorylated. Thus, VDAC2 met the criteria expected for a regulator of Bid dependent mitotic priming. The three mammalian isoforms of VDAC, show high sequence similarity, but appear to have distinct roles. VDAC1 is 10-fold more abundant than VDAC2, but was not significantly enriched in our BioID samples. Functional validation, performed by deleting VDAC2 in an

independent cell line (MCF7) from the screen, uncoupled mitotic priming from Bid phosphorylation. Interestingly, Bid was still phosphorylated in mitotic VDAC2 ko MCF7 cells, indicating that VDAC2 function lies downstream of potential regulatory kinases. Furthermore, loss of VDAC2 did not simply make the cells refractory to apoptosis, as the response of the VDAC2 ko cells to taxol was restored to the level of WT cells by ABT-737 treatment. Thus, at least in our model, VDAC2 is not essential for mitochondrial apoptosis.

Several previous studies have linked VDAC2 to Bak and Bax dependent apoptosis, but its precise role still remains unclear, and the functional consequences of its interactions in cells are disputed. Chemical cross-linking *in situ* identified VDAC2 as interacting with the inactive form of Bak. This interaction with VDAC2 suppressed mitochondrial Bak oligomerisation and activation [31]. Conversely, other studies found that the targeting of Bak to mitochondria required VDAC2 [43,44], and loss of this targeting function resulted in the inability of tBid to activate Bak. A genome-wide CRISPR/Cas9 screen in Mcl-1 deficient MEFs recently identified VDAC2 as a mediator of Bax, but not Bak, dependent apoptosis. Although both pro-apoptotic proteins could bind VDAC2, it was only required for Bax dependent death. However, an earlier study from the same group found that although loss of VDAC2 reduced both Bax and Bak mitochondrial association, they both retained the ability to kill cells in response to an apoptotic signal[34]. Finally, Bax retrotranslocation off mitochondria also requires VDAC2[33]. The details of these studies, often contradictory, probably reflect varying genetic backgrounds and cell types. However, it is clear that VDAC2 is emerging as a nexus of Bcl-2 protein coordination on mitochondria.

Knock out studies in mice support the idea that the function of VDAC2 in apoptosis regulation is influenced by the genetic and cellular context. Deletion of VDAC2 was originally reported to be embryonic lethal. VDAC2 -/- MEFs isolated from these mixed genetic background mice showed increased susceptibility to Bak activation. In support of these findings, a subsequent thymus specific VDAC2 knock out resulted in increased thymocyte apoptosis, which was rescued by deletion of Bak. However, a recent CRISPR generated deletion of VDAC2 in an inbred mouse line did not result in either unrestrained Bak activation or loss of embryonic viability, although the resulting mice failed to thrive for reasons more related to VDAC2's role in metabolite transport.

Our data here show that the absence of VDAC2 dampens mitotic priming to the same extent as loss of Bid or the ability to phosphorylate Bid. Furthermore, the dual loss of Bid function in mitosis and VDAC2 was not additive, showing that the priming effect of Bid phosphorylation was mediated by VDAC2. VDAC2 therefore appears to coordinate Bid in the context of a sensitizer BH3-protein, temporally adjusting mitochondrial priming in mitosis. Bid, along with Bim and Puma, are defined as direct activator BH3-proteins[38]. Bid as an activator is largely based on its function downstream of caspase 8 cleavage [39]. However, full-length Bid undergoes reversible post-translational modifications [40,41]. It is interesting to speculate that a significant role for Bid may be aligned with sensitisation in response mitosis. Notably, perturbing Bid function or S66 phosphorylation did not alter normal cell cycle progression, just the outcome following delayed mitotic exit.

BioID is a powerful approach that has potential for further dissecting the interactions of Bid and other Bcl-2 proteins in live cells. In this regard, we identified other potential candidates for novel interaction partners of Bid, including kinases, phosphatases and their regulatory subunits. One issue was that some of these proteins were identified through a small number of peptides in two out of three repeats. Whereas it is possible that some of these are real interactions, all need further validation beyond the scope of the present study. We were also surprised that we did not detect significant levels of other Bcl-2 proteins, particularly anti-apoptotic partners for Bid. We did isolate biotin labelled venus-Bcl-XL when it was co-expressed with the activator tBid-BirA*, and detected Bax and Bcl-XL in the stable HeLa lines in two out of three repeats. However only a small number of unique Bax peptides were detected, making quantitative comparisons between conditions unreliable. Despite this, we observed that Bax, was enriched in the presence of mBidWT but not mBidG94E, suggesting we were observing a BH3-domain dependent interaction. However, the fact that we didn't detect other Bcl-2 family partners remains apparent. Perhaps intermediate scaffold proteins such as VDAC2 are more readily labelled *in situ.* It will be interesting to see whether other Bcl-2 proteins also interact with similar scaffold proteins.

Finally, these results add to our understanding of how cells coordinate the dynamic changes in priming as they progress through mitosis. As with studies on VDAC, studies on mitotic cell death have variously implied significant roles for different

specific BH3-proteins, Bak or Bax. A genome-wide screen in HeLa cells identified Bax as key for taxol mediated cell death, whereas the same approach in RKO cells did not directly identify any Bcl-2 proteins, but instead myc dependent transcription of Bid, BIM and Noxa. An siRNA approach in HeLa cells specifically targeted at Bcl-2 proteins identified roles for Noxa and Bim in conjunction with Mcl-1 loss. Together, these studies indicate that the outcome of delayed mitotic exit is not determined by a specific BH3-protein or multi-domain effector, but rather a complex interplay of many, the balance of which will vary between cell and tissues types. Indeed, our data show that the relative contribution of Bid phosphorylation varies between breast cancer lines. MCF7 cells appear to have a prominent role for Bid phosphorylation in mitosis associated priming. In contrast, MDA-MB-231 cells appear to have a priming landscape distinct to that of MCF7, even though they still show mitosis specific phosphorylation of Bid. Using new approaches like BioID based proteomics will add new details to the way in which cells are coordinating dynamic changes in mitochondrial priming, and lead to the development of new strategies to manipulate these events for therapeutic purposes.

## Methods

*Cell culture.*

MCF-7, BT-474, MDA-MB-231, SK-BR-3, MCF-10A, HEK-293T, and HeLa cells were acquired from ATCC (American Type Culture Collection). MCF-10A cells were grown in DMEM-F12 supplemented with 5% horse serum (v/v), 100 ng/ml cholera toxin, 20 ng/ml epidermal growth factor, 0.5 g/ml hydrocortisone, 10 mg/ml insulin, 100 U/ml penicillin and 100 mg/ml streptomycin. HeLa cells were grown in EMEM supplemented with 10% foetal bovine serum (v/v), 100 U/ml penicillin and 100 mg/ml streptomycin. All other cell lines were cultured in DMEM supplemented with 10% foetal bovine serum (v/v), 100 U/ml penicillin and 100 mg/ml streptomycin.

*Single cell fate tracking.*

1 μM Taxol (Sigma-Aldrich), 5 μM ABT-737 (Sigma-Aldrich) or DMSO diluted in complete growth media was added to cells 30 minutes prior to imaging. Images were acquired at 15 minute intervals for 48-60 hours on an AS MDW live cell imaging system (Leica) in bright-field using a 20x objective and utilising imaging software Image Pro 6.3 (Media Cybernetics Ltd). Point visiting was used to allow multiple positions to be imaged within the same time course and cells were maintained at 37°C and 5% $CO_2$. Image stacks were analysed in ImageJ (National Institutes of Health), where single cells were identified and followed manually using cellular morphology to determine cell cycle progression and fate. Cells were described as being in mitosis from the initial point at which a cell began to round, till the first frame of cytokinesis or membrane blebbing. Cells that exhibited morphology associated with apoptosis such as membrane blebbing, shrinking of cell body, and in the later stages the formation of apoptotic bodies or secondary necrosis were described as having undergone apoptosis in mitosis [38]. Cells that exited mitosis as a single cell, or as two or more non-identical daughter cells were grouped together under the definition of having undergone mitotic slippage [3].

*Antibodies, immunofluorescnce and immunoblotting*.

The following antibodies were used for immunoblotting and immunoflourescence: rabbit anti-Bid (ProteinTech, #10988-1-AP); mouse anti-Myc ( Millipore, #05-724); rabbit anti-V5 (Sigma-Aldrich, # V8157); mouse anti-mtHsp70 (Thermo, # MA3-028); rabbit anti-GFP (Invitrogen, # PA1-9533); goat anti-β-actin (Abcam, # Ab8229); rabbit anti-phospho-Histone serine10 (Millepore, #06-570); mouse anti-vinculin (Abcam, # Ab9532). To detect biotinylated proteins we used DyLight 549 Streptavidin (Vector laboratories, # SA-5549) and IRDye680 Strepavidin (LiCor, #925-68079).

Immunofluorescent staining of cells was performed as previously described [39], using Alexafluor 594 and 488 conjugated secondary antibodies (Stratech). Immunostained cells were visualised using a Zeiss AxioImager M2 florescence microscope with 63x (NA 1.4) PLAN-APOCHROMAT objective. Images were acquired with Micro-Manager software and processed using ImageJ.

For immunoblotting, proteins were separated by SDS-PAGE and transferred to nitrocellulose. Following incubation with primary antibodies, proteins were detected using IrDye 800 and 680 secodary antibodies and an Odyssey CLx imager (LiCor). Quantification of blots was performed using ImageStudio (LiCor).

*Mitotic enrichment of cultured cells.*

Asynchronous cell populations were treated with nocodazole (Sigma-Aldrich, 200 ng/mL in complete growth media) for 16 hours to arrest cell in mitosis. Mitotic cells were then dislodged from the cell culture dish by tapping the vessel laterally against the bench. Media containing dislodged mitotic cells was removed and centrifuged at 350 RCF for 5 minutes to pellet cells ready for subsequent analysis.

*Flow cytometry analysis of cell cycle.*

Cell cycle distribution within a population was quantified by DNA content. Cycling cells were fixed with 70% ethanol and stained with DAPI. Stained cell samples were analysed on a BD Biosciences Fortessa flow cytometer, using Diva Version 8 (BD Biosciences) to collect raw data. Raw data was then analysed using Modfit LT (Version 5, Verity Software House) to quantify distribution between cell cycle phases.

*BioID mediated proximity labeling.*

For small scale assays such as Western blotting or immunofluorescent staining, cells expressing BirA* fusion proteins were seeded in a 6 well plate to approximately 80% confluence on day of labelling. Growth media was replaced with complete growth media supplemented with 50 μM biotin (Sigma-Aldrich), and cells cultured for a further 16 hours. Following incubation, biotin supplemented media was removed and replaced with regular growth media for 1 hour. Cells were then washed three times in PBS and assayed as appropriate.

For mass spectrometry experiments, cells expressing BioID fusion proteins were seeded into two 100 mm diameter dishes to be approximately 80% confluent next day. On the day of labelling, growth media was replaced with complete growth media supplemented with 50 μM biotin (Sigma-Aldrich) and cultured for a further for 16 hours, along with any other drug treatments. Following incubation, biotin supplemented media was removed and replaced with regular growth media for 1 hour to allow free biotin to diffuse out of cells. Cells were then washed three times in PBS and lysed in RIPA supplemented with 1x protease inhibitor cocktail (Millipore), 100 mM $Na_3VO_4$ and 500 mM NaF. Following lysis, lysates from both dishes were pooled, protein concentration measured and biotinylated proteins isolated via streptavidin-bead purification.

*Streptavidin affinity purification.*

Biotinylated proteins were isolated using MagReSyn® streptavidin (MagReSyn®). 100 μL of bead slurry was decanted into a microcentrifuge tube and exposed to a magnetic field to separate the liquid and bead phases. The liquid phase was discarded and beads were washed three times in ice-cold lysis buffer. Appropriate volumes of cell lysate were added to beads to yield 1 mg of total protein, and the volume made up to a total of 1 mL with lysis buffer. Lysates and beads were incubated overnight at 4°C on an end-over-end tumbler. The next day beads were collected, washed twice in lysis buffer, once in urea wash buffer (2 M urea, 10 mM Tris-HCl pH 8.0), then three more times with lysis buffer. Following the final wash, beads were resuspended in 100 μL 1x lithium dodecyl sulphate sample buffer (Novex NuPAGE) supplemented with 2 mM biotin and 50 mM dithiothreitol (DTT) and incubated at 95°C for 5 minutes to elute bound

proteins. Following elution, beads were collected and concentrated to 50 μL in a vacuum concentrator. 45 μL of sample was immediately subjected to SDS PAGE and processed for digestion in preparation for mass spectrometry, while the remaining 5 μL was analysed *via* western blotting to confirm biotinylation and protein enrichment.

*Mass spectrometry and protein identification.*

Affinity purified biotinylated proteins samples were briefly separated by SDS PAGE, then fixed and stained using InstantBlue (Expedeon). Gel fragments containing protein samples were digested with trypsin and peptides extracted under standard conditions [40]. Peptides were subjected to liquid-chromatography tandem mass spectrometry (LC-MS/MS) using a Thermo Orbitrap Elite coupled with a Thermo nanoRSLC system (Thermo Fisher Scientific). Peptides were selected for fragmentation automatically by data dependent analysis. Raw data was processed using Progenesis QI (v4.1, Nonlinear Dynamics) and searched against the SwissProt and Trembl databases (accessed July 2017). Database searches were performed against the human, mouse and *E. coli* proteome databases with tryptic digest specificity, allowing a maximum of two missed cleavages, and an initial mass tolerance of 5 ppm (parts per million). Carbamidomethylation of cysteine was applied as a fixed modification, while N-acylation and oxidation of methionine, as well as the biotinylation of lysine, were applied as variable modifications during the database searches.

*Label free protein quantification and data analysis.*

Relative label free protein quantification of mass spectrometry experiments was performed using Progenesis QI (v4.1, Nonlinear Dynamics). Raw data was processed and aligned in Progenesis QI. Once aligned, relative protein quantification was calculated from the abundances of ions with three or more isoforms identified as being from unique (non-conflicting) peptides. Comparisons between relative protein abundances were made between proteins isolated from wild type or mutant Bid-BirA* lysates (sample) and proteins isolated from venus-BirA* lysates (control) to calculate a fold change enrichment. Sample and control protein abundances were paired based on drug treatment, e.g. WTBid-BirA* +

nocodazole was compared with venus-BirA* + nocodazole. Statistical analysis of proteomics data was performed in Progenesis QI using ANOVA.

*VDAC2 deletion by CRISPR/Cas9.*

Deletion of endogenous *VDAC2* was achieved through CRISPR/Cas9 as described [41]. Two sgRNA sequences (CAATGTGTATTCCTCCATC, GATGGAGGAATACACATTG) designed to target upstream of the second protein coding exon were cloned into PX458 (pSpCas9(BB)-2A-GFP). PX458 containing the VDAC2 targeting guides was transfected into low passage WT MCF-7 cells and sorted by FACS for GFP expression. Single cells were isolated from the sort and plated into individual wells of 96 well plates. Wells in which clonal cell populations had expanded were transferred to larger cultures and genomic DNA extracted for identification of indels by PCR and sequencing.

*Statistical analysis.*

Details of statistical tests are provided in figure legends. Statistical analysis was performed using GraphPad Prism v7.

**Acknowledgements**.

RP was generously supported by a studentship funded by John and Janet Hartley. LK was funded through the Manchester Cancer Research Centre by a CRUK training award. JS was funded by a Biotechnology and Biological Sciences Research Council (BBSRC, UK) David Phillips Fellowship (BB/L024551/1). VM was partially supported by a grant from the Sir Richard Stapley Educational Trust. The Wellcome Centre for Cell-Matrix Research is supported by a core grant from the Wellcome Trust (203128/Z/16/Z). We are grateful for the assistance provided by staff in the bioimaging and proteomics core facilities.

**Author contributions**.

RP and APG conceived and planned the project. RP conducted the majority of the experiments presented in the paper. LK conducted apoptosis assays. VM and JS

assisted with the analysis of the MS data. PW generated the shBid virus constructs. LK, KB and JS carried out data analysis. RP and APG wrote the paper and all authors discussed the results and commented on the manuscript.

## Figure legends

**Figure 1.** *Human breast cell lines display heterogeneous responses to taxol induced prolonged mitosis.*

A. Single cell fate profiles of indicated human breast cell lines treated with 1μM taxol over a 60 hour period. Each individual horizontal line represents a single cell. Data represents 60 cells tracked over 2 independent repeats.

B. Summary of cell fate profiles from A after 60 hours.

C. Quantification of apoptosis in mitosis for the data in A. Error bars represent SD.

D. Duration of time in mitosis for the cells in A, all fates included. Mean and SD plotted

E. Cell lines were transiently transfected with mBid-GFP, then enriched for mitosis by overnight treatment with nocodazole followed by shake off. Whole cell lysates were then immunoblotted (IB) with the indicated anti-bodies. β-actin serves as loading control, while phospho-Histone H3 (pH3) indicates mitosis.

**Figure 2**. *Phosphorylation of Bid regulates apoptotic priming in mitotic breast cancer cells.*

A. MCF-7 cell lines were generated stably expressing either shBid alone or with the indicated mouse Bid-GFP variant (BidWT-GFP, BidS66A-GFP, BidG94E-GFP). Cells were either untreated or enriched for mitosis with 18 hour treatment in nocodazole followed by shake off. Whole cell lysates were immunoblotted with the indicated antibodies. Vinculin serves as loading control, while phospho-Histone H3 (pH3) indicates mitosis.

B. LiCor Odyssey quantification of human Bid (hBid) knock down and mouse Bid (mBid) expression in the lysates from A. Intensities were quantified and normalised to the vinculin loading control. Data from WT MCF7 and MCF7 mBidWT-GFP cells that had not undergone mitotic isolation are displayed. hBid expression was reduced by ~ 75% in shBid expressing lines.

C. Single cell fate profiles of the MCF-7 lines in A, untreated or treated with 1μM taxol over 50 hours. Data represents 90 cells tracked over 3 independent experiments.

D. Single cell fate profiles of the MCF-7 lines, untreated or treated with 1μM taxol, in the presence of 5μM ABT-737 over 50 hours. Data represent 90 cells tracked over 3 independent experiments.

E. Summary of apoptosis in mitosis for the data in C and D. Error bars represent SD

F. Summary of duration of mitosis, all fates included, for the data in C and D. Mean and SD plotted. For panels E & F data were analysed by one-way ANOVA, followed by Tukey's multiple comparison test (ns - non-significant; *** - $p<0.001$; **** - $p<0.0001$).

**Figure 3**. *Generation and validation of a Bid-BirA* bait fusion protein.*

A. Schematic diagram of BioID labelling strategy. Selective biotinylation of proximal proteins is followed by stringent cell lysis and streptavidin affinity purification.

B. HEK-293T cells were transiently transfected with plasmids expressing either tBid-eYFP, tBid-BirA* or Venus-BirA*. After an overnight incubation cells were harvested, cytospun onto slides and stained for their respective fusion proteins tag, eYFP, venus or myc (present on the Bid-BirA*). Apoptosis was quantified by nuclear fragmentation. Data represents mean and SD of 3 independent experiments. Data analysed by one-way ANOVA, followed by Tukey's multiple comparison test. **** represents $p <0.0001$. Scale bar = 10μm.

C. HEK293T cells transiently expressing tBid-BirA* or BirA* alone were incubated overnight in the presence or absence of biotin. In the presence of biotin tBid-BirA* and BirA* are seen to self-label at the predicted molecular weights. Endogenously biotinylated proteins are detected at around 280, 130, 76 and 74 kDa.

D. HEK-293T cells were transfected with plasmids expressing either GFP-Bcl-XL, or GFP-Bcl-XL and tBid-BirA*, then incubated overnight in the presence of biotin. Biotin

labelled proteins were isolated from whole cell lysates on streptavidin beads, separated by SDS-PAGE and immunoblotted for either GFP or biotin.

E. HEK-293T cells transfected and treated as in C. were fixed and immunostained for the myc-tag and biotin. Scale bar = 10μm.

**Figure 4**. *Mass spectrometry screen identifies VDAC2 as showing pBid dependent enrichment*

(A) Schematic diagram of mass spectrometry screen experimental design

(B) HeLa cells stably expressing BirA* fusion proteins were induced to label in the presence or absence of nocodazole.

(C) Volcano plot of mean fold change of biotinylated protein abundance for BidWT vs. Venus control for unsynchronised and nocodazole arrested samples. Positive ratio indicates enrichment in BidWT sample. P Value calculated via ANOVA.

(D) VDAC2 is identified as having high sequence coverage, and in low percentage of CRAPome experiments.

(E) Protein abundance fold change for VDAC2, mtHSP70 and DDX3X. Data represents mean and SD of 3 independent repeats. Significance calculated by unpaired t Tests, * $P<0.05$, ** $P<0.01$

**Figure 5.** *VDAC2 is a coordinator of pBid dependent apoptotic priming in mitosis.*

(A) Left hand panel - agarose gel electrophoresis of 300 bp PCR product at VDAC2 CRISPR target PAM site. Right hand panel - table displaying indels caused by CRISPR/Cas9 determined by DNA sequencing.

(B) Single cell fate profiles of MCF-7 VDAC2 KO lines in A, untreated or treated with 1μM taxol over 48 hours. Data represents 90 cells tracked over 3 independent experiments.

(C) D11 VDAC2 KO cells stably expressing VDAC2-V5 were fixed and immunostained for V5. Scale bar = 10µm.

(D) D11 VDAC2 KO MCF-7 cell lines were generated stably expressing VDAC2 V5, shBid alone or shBid in conjunction with the indicated mouse Bid-GFP variant (BidWT-GFP, BidS66A-GFP, BidG94E-GFP). Cells were either untreated or enriched for mitosis with 18 hour treatment in nocodazole followed by shake off. Whole cell lysates were immunoblotted with the indicated antibodies. β-actin serves as loading control, while phospho-Histone H3 (pH3) indicates mitosis.

(E) Summary of apoptosis in mitosis for single cell fate analysis of lines in D, untreated or treated with 1µM taxol and/or 5 µM ABT-737 over 48 hours (S5). Data represents 90 cells tracked over 3 independent experiments. Error bars represent SD Data analysed by one-way ANOVA, followed by Tukey's multiple comparison test. Ns represents non-significant, ** represents $p < 0.01$, *** represents $p < 0.001$.

**Table 1.** *Summary of enrichment data of three independent experiments for BidWT-BirA* relative to venus-BirA*.* Proteins are ordered by mean enrichment (Log2 ratio BidWT-BirA* vs. venus-BirA*). Only protein enriched in all three repeats are shown. Those highlighted in orange have CRAPome scores greater than 20%. VDAC2 is highlighted in red. Bid (highlighted in green) is the mouse protein used as bait. (A) Proteins enriched in unsynchronised HeLa cells. (B) Protein enriched in nocodazole treated HeLa cells.

## References


1 Tait, S. W. & Green, D. R. Mitochondria and cell death: outer membrane permeabilization and beyond. *Nat Rev Mol Cell Biol* **11**, 621-632, doi:10.1038/nrm2952 (2010).

2 Rehm, M. *et al.* Single-cell fluorescence resonance energy transfer analysis demonstrates that caspase activation during apoptosis is a rapid process. Role of caspase-3. *J Biol Chem* **277**, 24506-24514, doi:10.1074/jbc.M110789200 (2002).

3 Gascoigne, K. E. & Taylor, S. S. Cancer cells display profound intra- and interline variation following prolonged exposure to antimitotic drugs. *Cancer Cell* **14**, 111-122, doi:10.1016/j.ccr.2008.07.002 (2008).

4 Spencer, S. L., Gaudet, S., Albeck, J. G., Burke, J. M. & Sorger, P. K. Non-genetic origins of cell-to-cell variability in TRAIL-induced apoptosis. *Nature* **459**, 428-432, doi:10.1038/nature08012 (2009).

5 Sarosiek, K. A. *et al.* Developmental Regulation of Mitochondrial Apoptosis by c-Myc Governs Age- and Tissue-Specific Sensitivity to Cancer Therapeutics. *Cancer Cell* **31**, 142-156, doi:10.1016/j.ccell.2016.11.011 (2017).

6 Certo, M. *et al.* Mitochondria primed by death signals determine cellular addiction to antiapoptotic BCL-2 family members. *Cancer Cell* **9**, 351-365 (2006).

7 Schellenberg, B. *et al.* Bax exists in a dynamic equilibrium between the cytosol and mitochondria to control apoptotic priming. *Mol Cell* **49**, 959-971, doi:10.1016/j.molcel.2012.12.022 (2013).

8 Montero, J. *et al.* Drug-induced death signaling strategy rapidly predicts cancer response to chemotherapy. *Cell* **160**, 977-989, doi:10.1016/j.cell.2015.01.042 (2015).

9 Ni Chonghaile, T. *et al.* Pretreatment mitochondrial priming correlates with clinical response to cytotoxic chemotherapy. *Science* **334**, 1129-1133, doi:10.1126/science.1206727 (2011).

10 Youle, R. J. & Strasser, A. The BCL-2 protein family: opposing activities that mediate cell death. *Nat Rev Mol Cell Biol* **9**, 47-59 (2008).

11 Chen, H. C. *et al.* An interconnected hierarchical model of cell death regulation by the BCL-2 family. *Nat Cell Biol* **17**, 1270-1281, doi:10.1038/ncb3236 (2015).

12 Pecot, J. *et al.* Tight Sequestration of BH3 Proteins by BCL-xL at Subcellular Membranes Contributes to Apoptotic Resistance. *Cell Rep* **17**, 3347-3358, doi:10.1016/j.celrep.2016.11.064 (2016).

13 Grabow, S. *et al.* Subtle Changes in the Levels of BCL-2 Proteins Cause Severe Craniofacial Abnormalities. *Cell Rep* **24**, 3285-3295 e3284, doi:10.1016/j.celrep.2018.08.048 (2018).

14 Pedley, R. & Gilmore, A. P. Mitosis and mitochondrial priming for apoptosis. *Biol Chem* **397**, 595-605, doi:10.1515/hsz-2016-0134 (2016).

15 Berndtsson, M. *et al.* Phosphorylation of BAD at Ser-128 during mitosis and paclitaxel-induced apoptosis. *FEBS letters* **579**, 3090-3094, doi:10.1016/j.febslet.2005.04.067 (2005).

16 Harley, M. E., Allan, L. A., Sanderson, H. S. & Clarke, P. R. Phosphorylation of Mcl-1 by CDK1-cyclin B1 initiates its Cdc20-dependent destruction during mitotic arrest. *Embo J* **29**, 2407-2420, doi:10.1038/emboj.2010.112 (2010).

17 Mac Fhearraigh, S. & Mc Gee, M. M. Cyclin B1 interacts with the BH3-only protein Bim and mediates its phosphorylation by Cdk1 during mitosis. *Cell Cycle (Georgetown, Tex.)* **10**, 3886-3896, doi:10.4161/cc.10.22.18020 (2011).
18 Moustafa-Kamal, M., Gamache, I., Lu, Y., Li, S. & Teodoro, J. G. BimEL is phosphorylated at mitosis by Aurora A and targeted for degradation by βTrCP1. *Cell Death Differ* **20**, 1393-1403, doi:10.1038/cdd.2013.93 (2013).
19 Terrano, D. T., Upreti, M. & Chambers, T. C. Cyclin-dependent kinase 1-mediated Bcl-xL/Bcl-2 phosphorylation acts as a functional link coupling mitotic arrest and apoptosis. *Mol Cell Biol* **30**, 640-656, doi:10.1128/MCB.00882-09 (2010).
20 Wang, P. *et al.* Phosphorylation of the proapoptotic BH3-only protein bid primes mitochondria for apoptosis during mitotic arrest. *Cell Rep* **7**, 661-671, doi:10.1016/j.celrep.2014.03.050 (2014).
21 Diaz-Martinez, L. A. *et al.* Genome-wide siRNA screen reveals coupling between mitotic apoptosis and adaptation. *Embo J* **33**, 1960-1976, doi:10.15252/embj.201487826 (2014).
22 Topham, C. *et al.* MYC Is a Major Determinant of Mitotic Cell Fate. *Cancer Cell* **28**, 129-140, doi:10.1016/j.ccell.2015.06.001 (2015).
23 Wertz, I. E. *et al.* Sensitivity to antitubulin chemotherapeutics is regulated by MCL1 and FBW7. *Nature* **471**, 110-114, doi:10.1038/nature09779 (2011).
24 Weaver, B. A. How Taxol/paclitaxel kills cancer cells. *Mol Biol Cell* **25**, 2677-2681, doi:10.1091/mbc.E14-04-0916 (2014).
25 Topham, C. H. & Taylor, S. S. Mitosis and apoptosis: how is the balance set? *Curr Opin Cell Biol* **25**, 780-785, doi:10.1016/j.ceb.2013.07.003 (2013).
26 Roux, K. J., Kim, D. I., Raida, M. & Burke, B. A promiscuous biotin ligase fusion protein identifies proximal and interacting proteins in mammalian cells. *J Cell Biol* **196**, 801-810, doi:10.1083/jcb.201112098 (2012).
27 Agircan, F. G., Hata, S., Nussbaum-Krammer, C., Atorino, E. & Schiebel, E. Proximity mapping of human separase by the BioID approach. *Biochem Biophys Res Commun* **478**, 656-662, doi:10.1016/j.bbrc.2016.08.002 (2016).
28 Dong, J. M. *et al.* Proximity biotinylation provides insight into the molecular composition of focal adhesions at the nanometer scale. *Sci Signal* **9**, rs4, doi:10.1126/scisignal.aaf3572 (2016).
29 Kim, D. I. *et al.* An improved smaller biotin ligase for BioID proximity labeling. *Mol Biol Cell* **27**, 1188-1196, doi:10.1091/mbc.E15-12-0844 (2016).
30 Hsu, Y. T. & Youle, R. J. Nonionic detergents induce dimerization among members of the Bcl-2 family. *Journal Of Biological Chemistry* **272**, 13829-13834 (1997).
31 Hsu, Y. T. & Youle, R. J. Bax in murine thymus is a soluble monomeric protein that displays differential detergent-induced conformations. *Journal of Biological Chemistry* **273**, 10777-10783 (1998).
32 Jeronimo, C. *et al.* Systematic analysis of the protein interaction network for the human transcription machinery reveals the identity of the 7SK capping enzyme. *Mol Cell* **27**, 262-274, doi:10.1016/j.molcel.2007.06.027 (2007).
33 Cheng, E. H., Sheiko, T. V., Fisher, J. K., Craigen, W. J. & Korsmeyer, S. J. VDAC2 inhibits BAK activation and mitochondrial apoptosis. *Science* **301**, 513-517, doi:10.1126/science.1083995 (2003).
34 Chin, H. S. *et al.* VDAC2 enables BAX to mediate apoptosis and limit tumor development. *Nat Commun* **9**, 4976, doi:10.1038/s41467-018-07309-4 (2018).

35 Lauterwasser, J. *et al.* The porin VDAC2 is the mitochondrial platform for Bax retrotranslocation. *Sci Rep* **6**, 32994, doi:10.1038/srep32994 (2016).

36 Ma, S. B. *et al.* Bax targets mitochondria by distinct mechanisms before or during apoptotic cell death: a requirement for VDAC2 or Bak for efficient Bax apoptotic function. *Cell Death Differ* **21**, 1925-1935, doi:10.1038/cdd.2014.119 (2014).

37 De Pinto, V. *et al.* Characterization of human VDAC isoforms: a peculiar function for VDAC3? *Biochim Biophys Acta* **1797**, 1268-1275, doi:10.1016/j.bbabio.2010.01.031 (2010).

38 Galluzzi, L. *et al.* Molecular mechanisms of cell death: recommendations of the Nomenclature Committee on Cell Death 2018. *Cell Death Differ* **25**, 486-541, doi:10.1038/s41418-017-0012-4 (2018).

39 Valentijn, A. J., Metcalfe, A. D., Kott, J., Streuli, C. H. & Gilmore, A. P. Spatial and temporal changes in Bax subcellular localization during anoikis. *J Cell Biol* **162**, 599-612 (2003).

40 Shevchenko, A., Tomas, H., Havlis, J., Olsen, J. V. & Mann, M. In-gel digestion for mass spectrometric characterization of proteins and proteomes. *Nat Protoc* **1**, 2856-2860, doi:10.1038/nprot.2006.468 (2006).

41 Ran, F. A. *et al.* Genome engineering using the CRISPR-Cas9 system. *Nat Protoc* **8**, 2281-2308, doi:10.1038/nprot.2013.143 (2013).

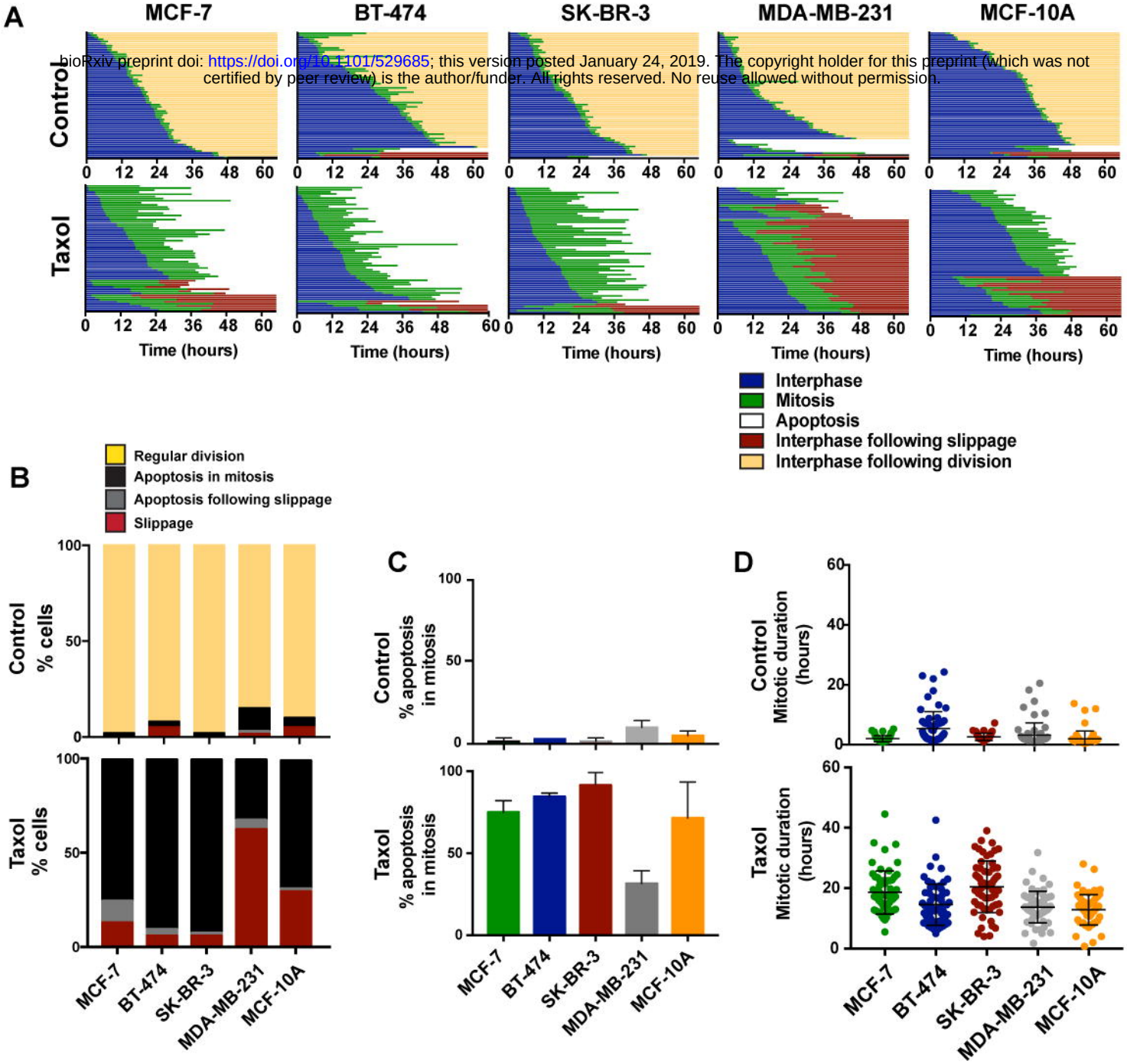


Pedley Figure 1

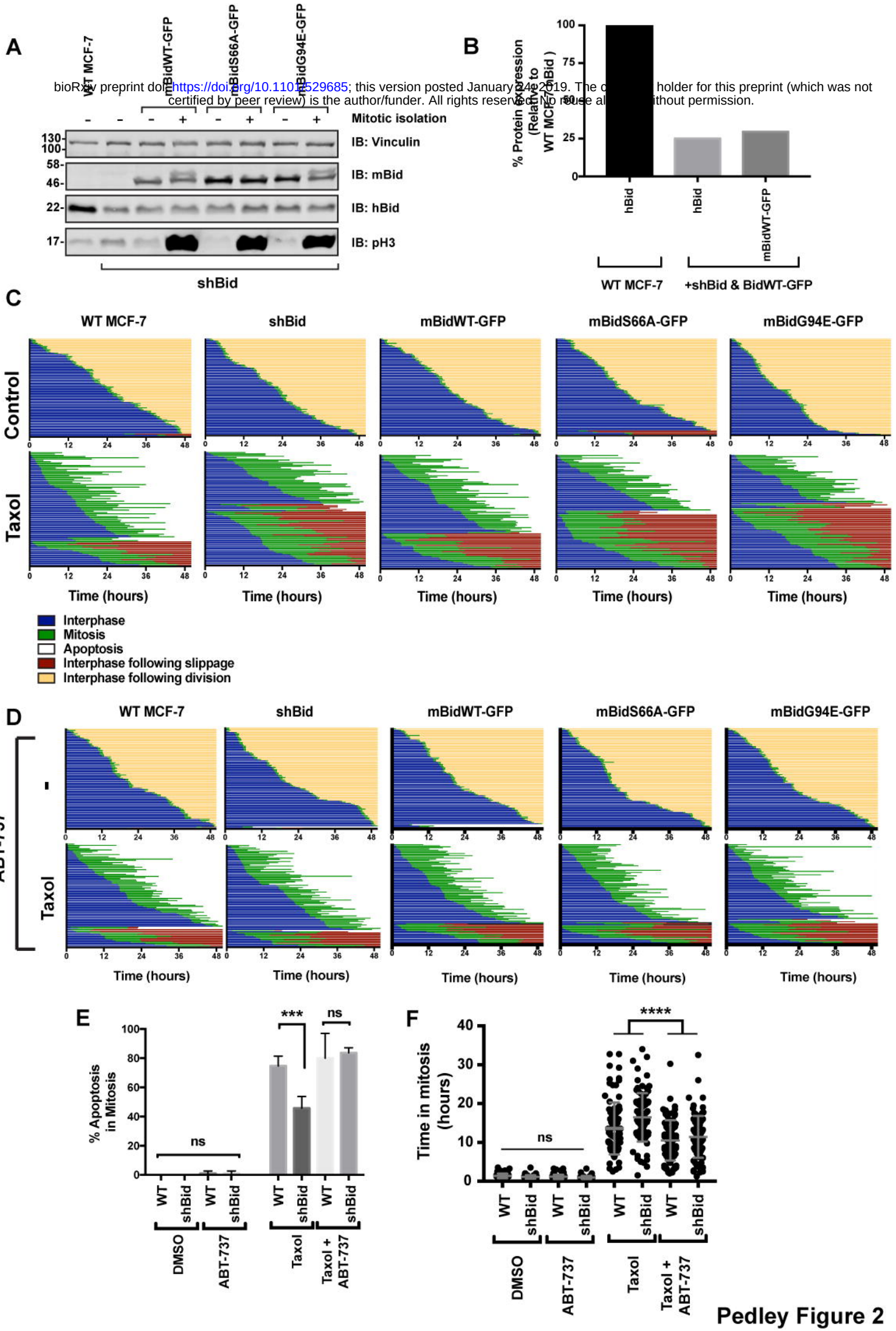


Pedley Figure 2

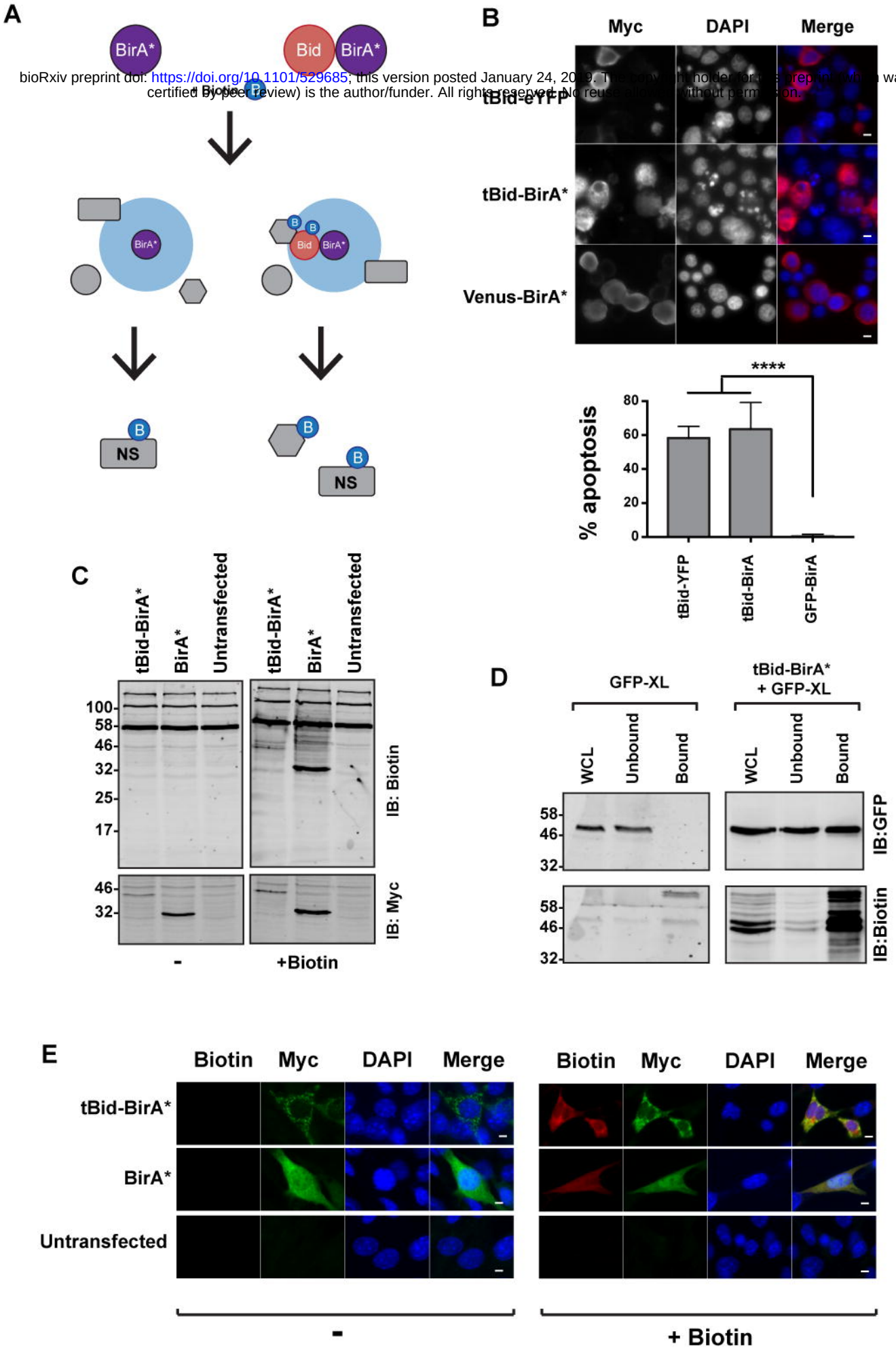


Pedley Figure 3

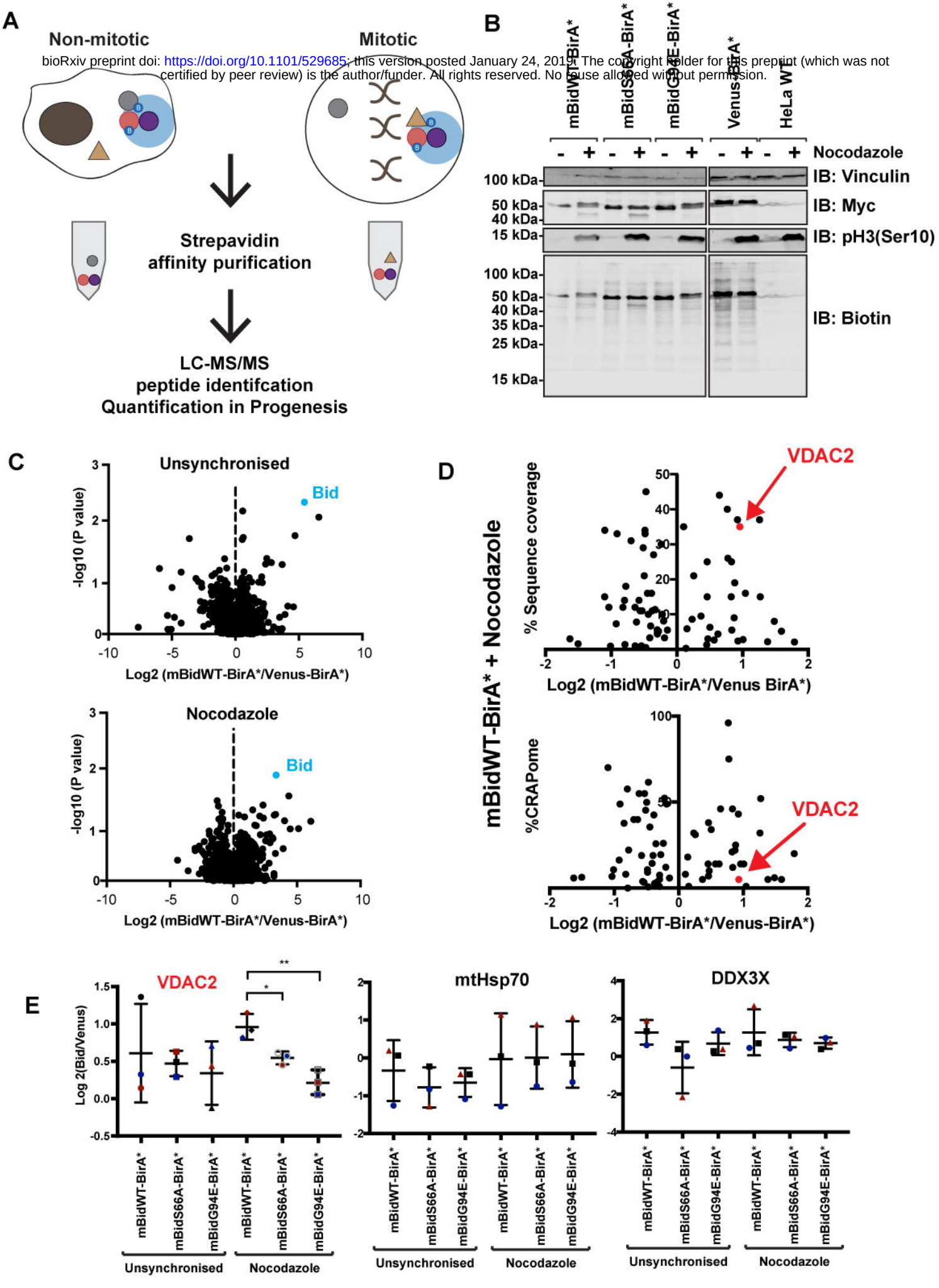


Pedley Figure 4

A

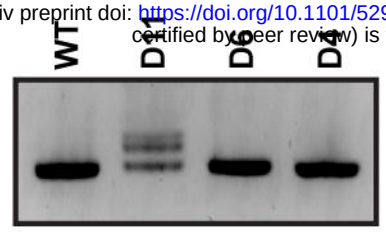


| | D11 | | D6 | | D4 | |
|---|---|---|---|---|---|---|
| Allele | Indel | Frame Shift | Indel | Frame Shift | Indel | Frame Shift |
| 1 | 287 bp insertion | Yes | 2 bp insertion | Yes | 1 bp insertion | Yes |
| 2 | 170 bp insertion | Yes | 1 bp insertion | Yes | 1 bp insertion | Yes |
| 3 | 1 bp insertion | Yes | WT | No | 3 bp deletion | No |

B

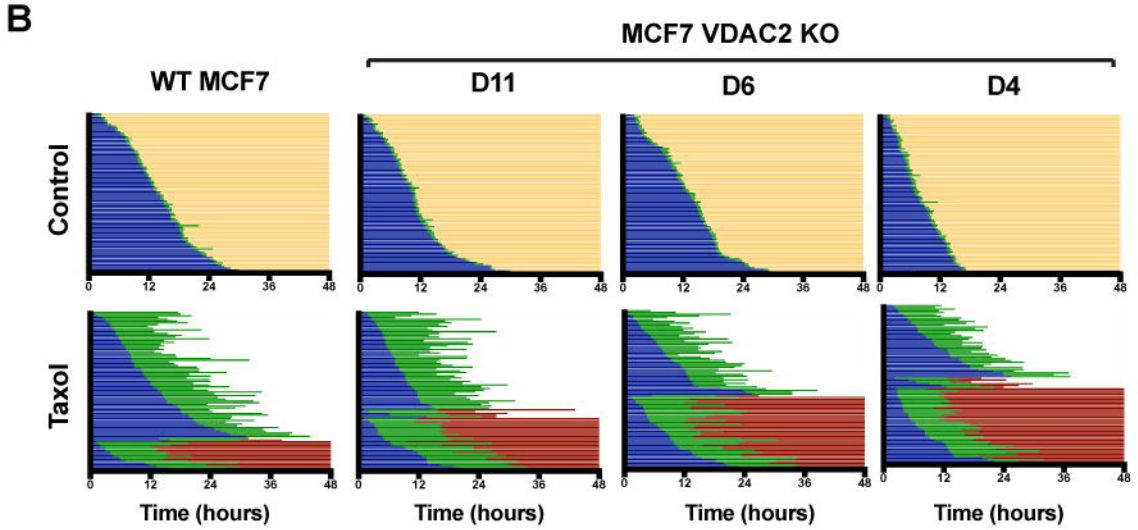


C

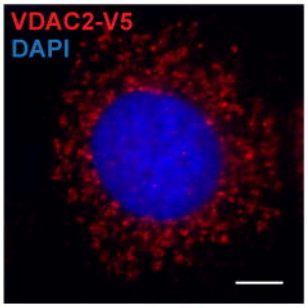


D

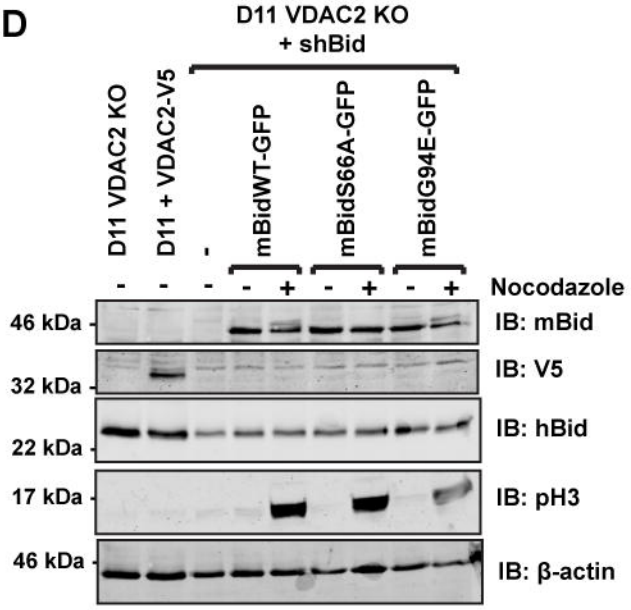


E

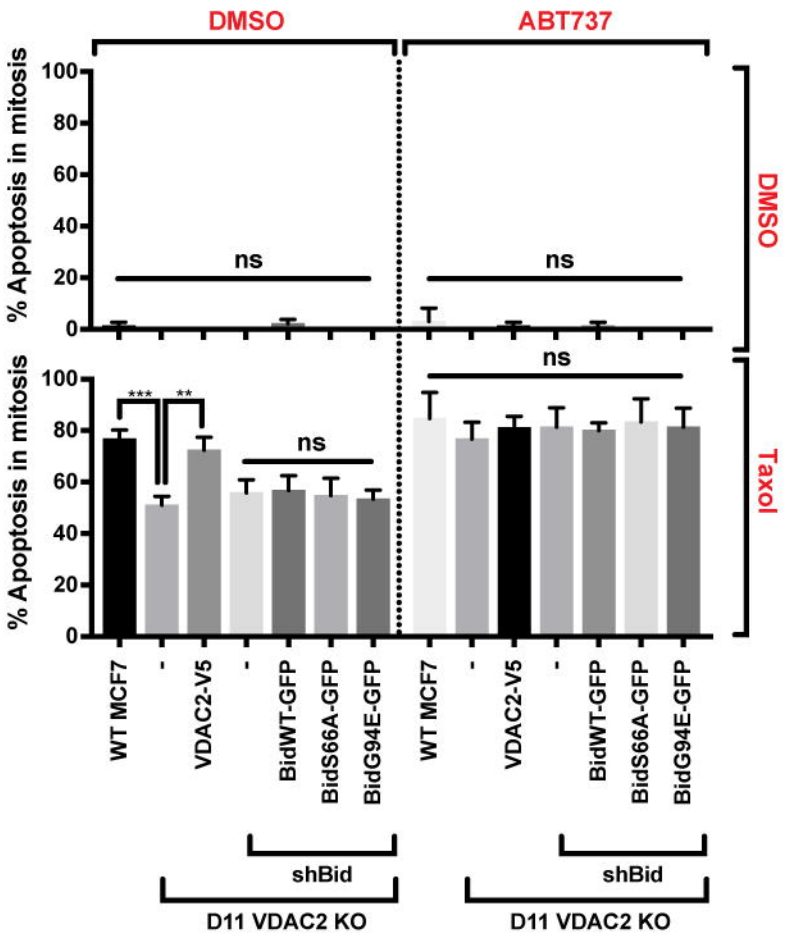


Pedley Figure 5

**A**

| Gene Name | Description/Protein name | CRAPome % | Sequence | Log2(ratio) R1 | R2 | R3 | Mean |
|---|---|---|---|---|---|---|---|
| BID | BH3-interacting domain death agonist (mouse) | 1.45985401 | N/A | 3.0938 | 3.7087 | 5.2609 | 4.0211 |
| DDX3X | ATP-dependent RNA helicase DDX3X | 51.5815085 | 25.0% | 0.5952 | 1.3268 | 1.8938 | 1.272 |
| HNRNPDL | Heterogeneous nuclear ribonucleoprotein D-like | 33.8199513 | 6.3% | 0.3617 | 0.4115 | 2.66 | 1.1444 |
| EIF4G1 | Eukaryotic translation initiation factor 4 gamma 1 | 24.8175182 | 14.0% | 2.4891 | 0.2486 | 0.6456 | 1.1278 |
| FLNC | Filamin-C | 35.7664234 | 4.4% | 0.0158 | 0.5413 | 2.1898 | 0.9156 |
| EIF4A1 | Eukaryotic initiation factor 4A-I | 46.2287105 | 45.0% | 0.2616 | 1.0855 | 1.327 | 0.8913 |
| CAND1 | Cullin-associated NEDD8-dissociated protein 1 | 21.4111922 | 6.3% | 0.1572 | 1.9041 | 0.55 | 0.8704 |
| XRN2 | 5'-3' exoribonuclease 2 | 23.6009732 | 2.9% | 0.5682 | 0.3794 | 1.4128 | 0.7868 |
| SEPT9 | Septin 9, isoform CRA_a | 19.2214112 | 35.0% | 0.309 | 1.4821 | 0.4482 | 0.7464 |
| SLC25A11 | Mitochondrial 2-oxoglutarate/malate carrier protein | 13.3819951 | 8.8% | 0.0728 | 0.7566 | 1.389 | 0.7395 |
| SON | Protein SON | 17.2749392 | 0.7% | 0.0687 | 0.3819 | 1.5642 | 0.6716 |
| RPA1 | Replication protein A 70 kDa DNA-binding subunit | 20.4379562 | 8.6% | 0.2333 | 0.4403 | 1.3284 | 0.6673 |
| RPN1 | Dolichyl-diphosphooligosaccharide--protein glycosyltransferase subunit 1 | 22.1411192 | 18.0% | 1.1139 | 0.4283 | 0.374 | 0.6388 |
| DSP | Desmoplakin | 30.6569343 | 17.0% | 0.5081 | 0.7725 | 0.5366 | 0.6057 |
| NAT10 | RNA cytidine acetyltransferase | 17.0316302 | 4.5% | 0.0914 | 0.6398 | 1.0533 | 0.5948 |
| VDAC2 | Voltage-dependent anion channel 2, isoform CRA_a | 14.1119221 | 49.0% | 0.1933 | 1.3612 | 0.1427 | 0.5657 |
| HUWE1 | HECT, UBA and WWE domain containing 1, isoform CRA_ | 18.0048662 | 0.3% | 0.3486 | 0.0866 | 1.1756 | 0.5369 |
| RBBP6 | E3 ubiquitin-protein ligase RBBP6 | 9.48905109 | 1.9% | 0.5828 | 0.313 | 0.6858 | 0.5272 |
| H2AFY | Histone H2A | 16.5450122 | 5.9% | 0.7703 | 0.304 | 0.3784 | 0.4843 |
| SFPQ | Splicing factor, proline- and glutamine-rich | 48.9051095 | 7.2% | 0.0703 | 0.6419 | 0.659 | 0.4571 |
| DYNC1H1 | Cytoplasmic dynein 1 heavy chain 1 | 31.8734793 | 3.1% | 0.0805 | 0.388 | 0.8726 | 0.447 |
| RPL23A | 60S ribosomal protein L23a (Fragment) | 54.5012165 | 20.0% | 0.0911 | 0.6077 | 0.5958 | 0.4315 |
| MAP4 | Microtubule-associated protein | 20.4379562 | 11.0% | 0.3446 | 0.7672 | 0.1653 | 0.4257 |
| STAT1 | Signal transducer and activator of transcription 1-alpha/beta | 5.59610706 | 12.0% | 0.0564 | 0.2314 | 0.8246 | 0.3708 |
| HSPA9 | Stress-70 protein, mitochondrial (Fragment) | 74.6958637 | 25.0% | 0.7743 | 0.0601 | 0.1959 | 0.3434 |
| PCBP2 | Poly(rC)-binding protein 2 (Fragment) | 45.9854015 | 26.0% | 0.125 | 0.7366 | 0.0591 | 0.3069 |
| DLST | Dihydrolipoamide S-succinyltransferase (E2 component of 2-oxo-glutarate complex) | 13.8686131 | 4.4% | 0.1503 | 0.2053 | 0.5323 | 0.296 |
| ABCD3 | ATP-binding cassette sub-family D member 3 | 9.7323601 | 3.5% | 0.0027 | 0.2813 | 0.5667 | 0.2835 |
| DKFZp686L20222 | Putative uncharacterized protein DKFZp686L20222 | 19.7080292 | 26.0% | 0.2651 | 0.2892 | 0.2908 | 0.2817 |
| CORO1B | Coronin | 9.24574209 | 38.0% | 0.0107 | 0.4157 | 0.3361 | 0.2542 |
| DNA helicase | DNA helicase | N/A | 11.0% | 0.274 | 0.2173 | 0.0469 | 0.1794 |
| PAICS | Multifunctional protein ADE2 | 25.7907543 | 40.0% | 0.1013 | 0.1215 | 0.2679 | 0.1636 |
| PRDX1 | Peroxiredoxin-1 | 61.5571776 | 45.0% | 0.0565 | 0.0192 | 0.2916 | 0.1224 |
| CSDE1 | Cold shock domain containing E1, RNA-binding, isoform CRA_a | 16.3017032 | 21.0% | 0.0637 | 0.2407 | 0.0214 | 0.1086 |
| HSPA1L | Heat shock 70 kDa protein 1-like | 94.6472019 | 43.0% | 1.0404 | 0.0366 | 0.4938 | 0.5236 |

**B**

| Gene Name | Description/Protein name | CRAPome % | Sequence | Log2(ratio) R1 | R2 | R3 | Mean |
|---|---|---|---|---|---|---|---|
| BID | BH3-interacting domain death agonist (mouse) | 1.45985401 | N/A | 2.4156 | 2.7285 | 4.0717 | 3.0719 |
| RPA1 | Replication protein A 70 kDa DNA-binding subunit | 20.4379562 | 2.1% | 0.1788 | 0.2281 | 4.9663 | 1.7911 |
| G6PD | Glucose-6-phosphate 1-dehydrogenase | 5.10948905 | 5.2% | 0.4457 | 0.0032 | 4.3265 | 1.5918 |
| FH | Fumarate hydratase isoform 1 | 5.83941606 | 8.0% | 0.3257 | 1.2192 | 2.9022 | 1.4824 |
| BRAP | BRCA1-associated protein | 4.62287105 | 2.2% | 0.4617 | 0.2416 | 3.4416 | 1.3816 |
| DDX3X | ATP-dependent RNA helicase DDX3X | 51.5815085 | 15.0% | 0.4491 | 0.6961 | 2.6677 | 1.2709 |
| MYH14 | Myosin-14 | 32.1167883 | 37.0% | 1.0245 | 0.0991 | 2.6563 | 1.26 |
| CAPG | Macrophage-capping protein | 1.21654501 | 16.0% | 1.0559 | 0.0608 | 2.0144 | 1.0437 |
| NCAPG | Non-SMC condensin I complex, subunit G | 14.3552311 | 2.8% | 0.822 | 0.0937 | 2.1065 | 1.0074 |
| VDAC2 | Voltage-dependent anion channel 2, isoform CRA | 14.1119221 | 35% | 0.8123 | 0.9139 | 1.1538 | 0.96 |
| LIMCH1 | LIM and calponin homology domains-containing protein 1 | 5.35279805 | 2.4% | 0.0679 | 0.1892 | 2.532 | 0.9297 |
| SLC25A31 | ADP/ATP translocase 4 | 42.8223844 | 37.0% | 0.0914 | 0.2876 | 2.3923 | 0.9238 |
| EIF4G1 | Eukaryotic translation initiation factor 4 gamma 1 | 24.8175182 | 19.0% | 0.4677 | 0.3714 | 1.8038 | 0.881 |
| ARCN1 | Archain 1, isoform CRA_b | 22.3844282 | 9.0% | 0.0957 | 0.208 | 2.3114 | 0.8717 |
| NUP155 | Nucleoporin 155kDa, isoform CRA_a | 11.9221411 | 5.5% | 0.647 | 0.0664 | 1.7934 | 0.8356 |
| PCBP2 | Poly(rC)-binding protein 2 | 45.9854015 | 25.0% | 0.7062 | 0.299 | 1.4907 | 0.832 |
| MCCC1 | Methylcrotonoyl-CoA carboxylase subunit alpha, mitochondrial | 21.4111922 | 15.0% | 0.0062 | 0.1132 | 2.367 | 0.8288 |
| HSPA9 | Stress-70 protein, mitochondrial | 74.6958637 | 26.0% | 1.1432 | 0.0402 | 1.1434 | 0.7756 |
| HSPA8 | Heat shock cognate 71 kDa protein | 96.350365 | 40.0% | 0.1977 | 0.2499 | 1.8551 | 0.7676 |
| EIF4A1 | Eukaryotic initiation factor 4A-I | 46.2287105 | 44.0% | 0.2503 | 0.8419 | 0.8524 | 0.6482 |
| DLST | Dihydrolipoamide S-succinyltransferase (E2 component of 2-oxo-glutarate complex) | 13.8686131 | 4.4% | 0.1382 | 0.3259 | 1.4145 | 0.6262 |
| CHD3 | Chromodomain-helicase-DNA-binding protein 3 | 13.6253041 | 2.7% | 1.2321 | 0.324 | 0.1461 | 0.5674 |
| HNRNPDL | Heterogeneous nuclear ribonucleoprotein D-like | 33.8199513 | 6.3% | 0.5105 | 0.3268 | 0.6739 | 0.5038 |
| AP3B1 | Adaptor-related protein complex 3 beta 1 subunit isoform 1 | 9.9756691 | 3.0% | 0.352 | 0.2181 | 0.849 | 0.473 |
| EPRS | Bifunctional glutamate/proline--tRNA ligase | 38.1995134 | 25.0% | 0.6685 | 0.1446 | 0.5679 | 0.4603 |
| EPS15L1 | Epidermal growth factor receptor substrate 15-like 1 | 6.56934307 | 15.0% | 0.402 | 0.1488 | 0.8297 | 0.4602 |
| CHD5 | Chromodomain-helicase-DNA-binding protein 5 | 14.1119221 | 1.3% | 0.1288 | 0.0948 | 1.137 | 0.4535 |
| AHNAK2 | Protein AHNAK2 | 4.86618005 | 9.5% | 0.3394 | 0.2897 | 0.4748 | 0.368 |
| DSP | Desmoplakin | 30.6569343 | 21.0% | 0.1322 | 0.3626 | 0.2722 | 0.2557 |
| PABPC3 | Polyadenylate-binding protein 3 | 31.6301703 | 8.6% | 0.1208 | 0.3089 | 0.2698 | 0.2332 |
| ABCF3 | ATP-binding cassette sub-family F member 3 isoform 1 | 0.72992701 | 5.9% | 0.1434 | 0.2088 | 0.111 | 0.1544 |
| HUWE1 | HECT, UBA and WWE domain containing 1, isoform CRA_b | 18.0048662 | 0.3% | 0.1824 | 0.0494 | 0.1844 | 0.1387 |
| PDLIM1 | PDZ and LIM domain protein 1 | 7.78588808 | 35.0% | 0.0294 | 0.1848 | 0.0953 | 0.1032 |

**Pedley Tabel 1**